Journal of Power Sources 268 (2014) 565–574

Contents lists available at ScienceDirect

Journal of Power Sources

journal homepage: www.elsevier.com/locate/jpowsour

The effects of moisture contamination in the Li-O_2 battery

M.H. Cho [a], J. Trottier [a], C. Gagnon [a], P. Hovington [a], D. Clément [a], A. Vijh [a], C.-S. Kim [a], A. Guerfi [a], R. Black [b], L. Nazar [b], K. Zaghib [a, *]

[a] Institut de Recherche d'Hydro-Québec (IREQ), 1800 boul. Lionel Boulet, Varennes, Québec J3X 1S1, Canada
[b] Department of Chemistry, University of Waterloo, 200 University Avenue West, Waterloo, Ontario N2L 3G1, Canada

HIGHLIGHTS

- Li-O_2 batteries have been tested under different atmospheres.
- Li-O_2 battery is very sensitive to even traces of moisture contamination.
- Moisture leads to higher capacity with serious impedance increase.

GRAPHICAL ABSTRACT

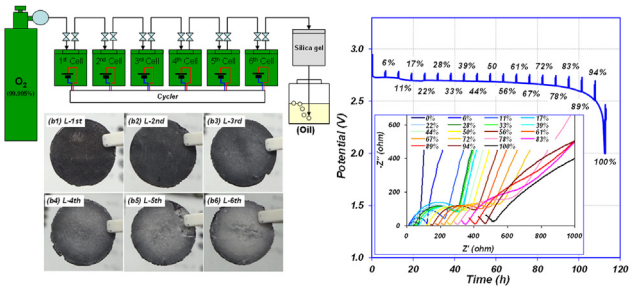

ARTICLE INFO

Article history:
Received 25 March 2014
Received in revised form
30 May 2014
Accepted 31 May 2014
Available online 10 June 2014

Keywords:
Li-O_2 battery
O_2 flow path
Lithium metal
Cycle life
Moisture contamination

ABSTRACT

The effects of moisture contamination in the Li-O_2 battery system were investigated by comparing the electrochemical performance and post-mortem analysis of batteries prepared under different atmospheres: sealed container in an ambient atmosphere *vs.* sealed container in a dry-room or in a glove-box. The performance of the cells strongly depended on the atmosphere; furthermore it was found that the performance degradation of the Li metal anode comes from moisture contamination from the feed lines. In an ambient atmosphere, the cells showed higher 1st discharge capacity, higher impedance and significant increase of the cell weight owing to contamination of the oxygen by moisture. Post-mortem analysis revealed that the deterioration of lithium metal anode leads to the cell failure mechanism, and this comes from the moisture contamination. It was found that the performance of Li-O_2 batteries is very sensitive to even traces of moisture contamination and every single part of the cell design including the choice of fitting parts and water permeability of the fitting material should be verified in order to obtain credible and reproducible results. This finding supports the idea that protection of the lithium metal electrode is indispensable to realize the practical application of Li-O_2 or Li-air batteries.

1. Introduction

The Li-air battery is considered one of the most desired technologies for electric vehicles because of its high theoretical specific energy (more than 3500 Wh kg^{-1}, including oxygen), which could enable a longer driving distance of >300 miles [1–3]. However, there are many technical challenges that hinder the practical use of lithium-air batteries. To address these technical challenges, significant research has been dedicated in the last 5 years on investigations of electrolytes [4–7], electrode materials and structures [8,9], catalysts [10–13], binders [14] and anodes [15,16]. Despite the significant progress in understanding the mechanisms associated with the electrode reactions, the current lithium-air technology is very far from the requirements

* Corresponding author.
E-mail address: zaghib.karim@ireq.ca (K. Zaghib).

http://dx.doi.org/10.1016/j.jpowsour.2014.05.148
0378-7753/

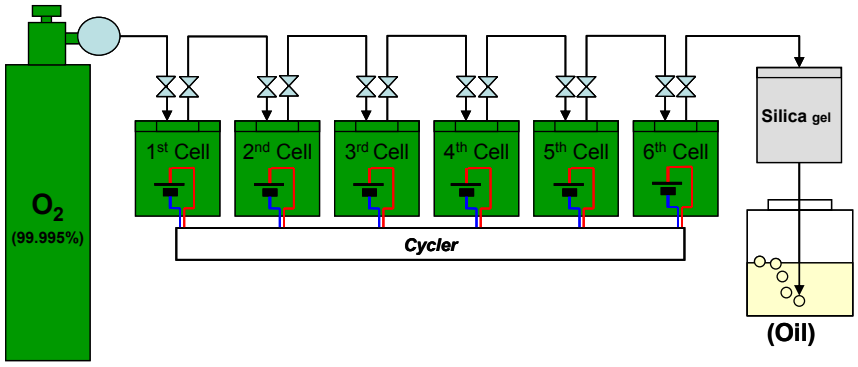

Fig. 1. Schematic diagram of O_2 flow and cell connections. O_2 line was serially connected from the 1st cell to the 6th cell through a single pathway while the individual cells were independently controlled by a cycler.

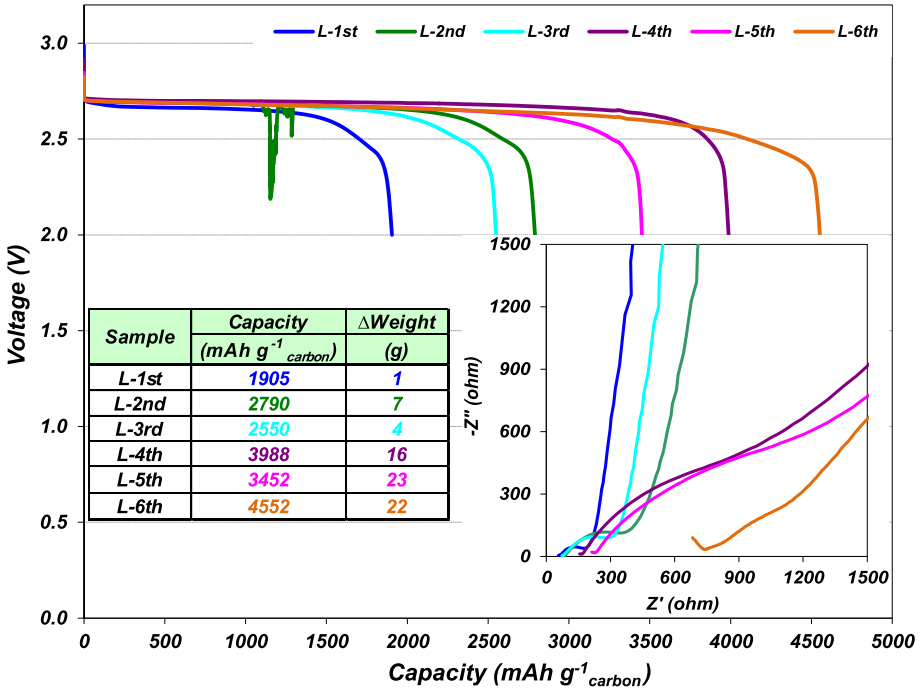

Fig. 2. The 1st discharge profiles according to the cell positions at a constant current of 50 mA g^{-1}_{carbon} between 2.0 and 4.3 V in sealed containers in ambient atmosphere. The impedance profiles, the discharge capacity and the cell weight change after discharge for each cell are displayed in the insets, which are significantly influenced by the connection order of the cells.

for use in electric vehicles, especially with respect to the cycle life and the power capability. Recently, some research groups have reported improvements extending to a few hundred cycles using a capacity or time controlled protocol [10,17], but the life is still limited to less than tens of cycles in the full operating voltage range (2.0–4.3 V).

In this work, we examine the effects of moisture contamination on the Li-O_2 battery. Although it is appreciated that the performance is profoundly sensitive to water, this study allows us to quantify the effects. It is found that the capacity and cell weight is significantly increased by even traces of H_2O contamination, leading to deterioration of the lithium metal (which serves as an indicator) and failure of the cell. It is also suggested that the seal-tightness should be well verified in all cell studies.

2. Experimental

2.1. Electrode preparation and cell assembly

Carbon black (Super-P, TIMCAL) was coated on carbon paper (TGP-H-030, Toray) and dried under vacuum at 100 °C for 24 h. The loading of carbon coating was controlled to *ca.* 0.4 mg cm^{-2} after drying. Commercially available coin-type cells (Hohsen, punched-CR2032) were assembled in a He filled glove box. Cathode electrodes with a 16 mm diameter were used. Lithium foil (Hohsen, 200 μm) was used as anode, and 3 layers of porous polypropylene (PP, Celgard 3501)/glass filter (GF/C, Whatman)/PP (Celgard 3501) separators were used to facilitate the recovery of the electrode after disassembly of the cells. The power performance was not deteriorated by the addition of two PP layers at

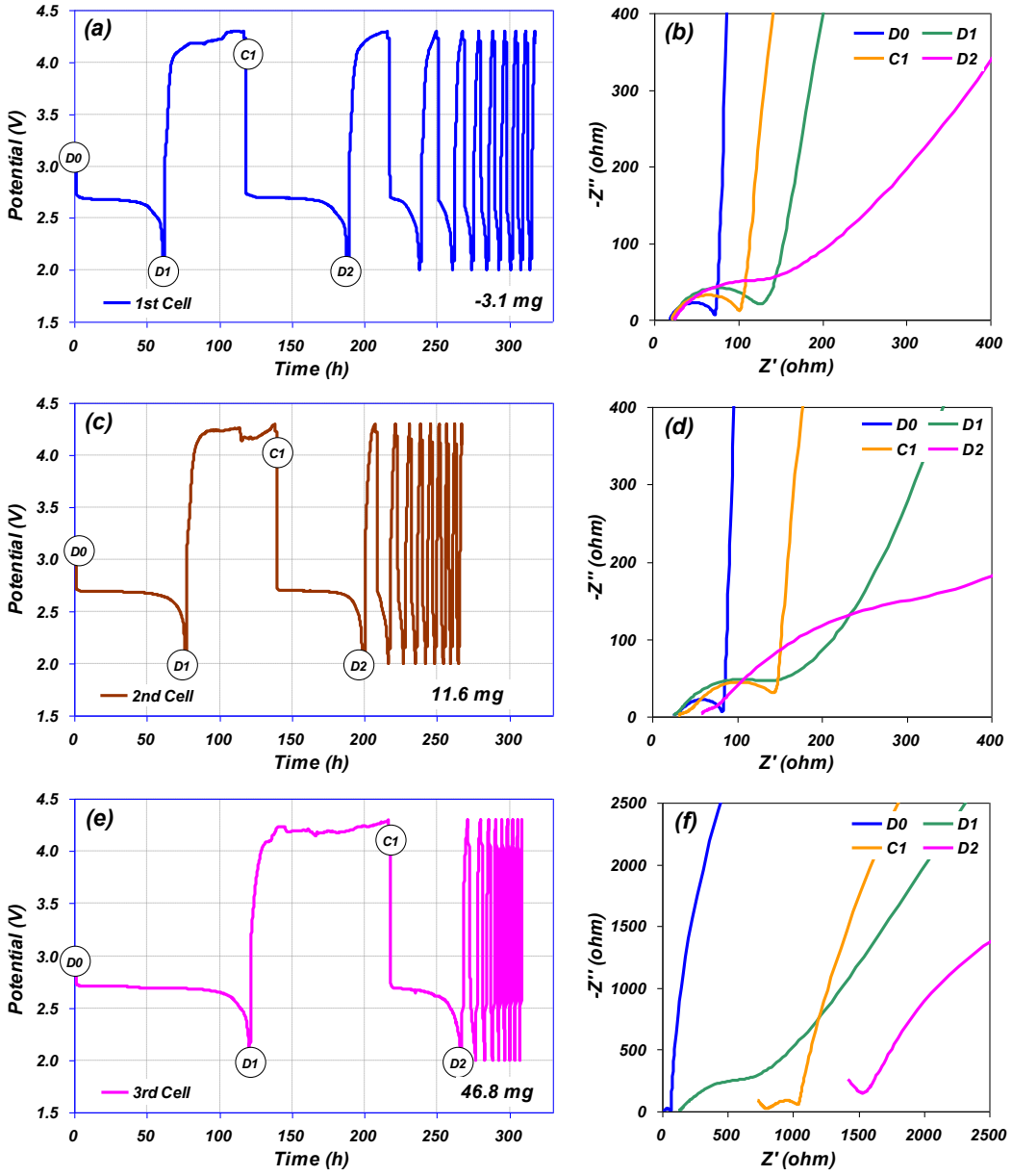

Fig. 3. Cycle behavior (a, c, e) and the relevant change of impedance spectra (b, d, f) according to the cell positions. (a) and (b) : the 1st cell, (c) and (d): the 2nd cell, (e) and (f) : the 3rd cell.

this low current rate of 50 mA g^{-1}_{carbon}. The electrolyte consisted of about 80 mg of $LiCF_3SO_3$ (lithium triflate, 99.995%, Sigma–Aldrich): TEGDME (tetraethylene glycol dimethyl ether, ≥99%, Sigma–Aldrich) by 1:4 mole ratios, which was injected into the cell after drying to have the moisture content of <20 ppm H_2O. The cell weight was monitored during electrolyte injection and the subsequent electrochemical tests.

2.2. Electrochemical tests and characterization

The coin cells were placed in the container (Bernardin, Mason Jar 250 ml with Standard 70 mm snap lid 1-PC) that has two fitting lines for gas inlet and gas outlet (Kimble Chase Life Science, Stopcock Nylon 3-way PK/10). Sealing resin (Torr Seal, Varian, Inc.) was applied on the joint parts to enhance the seal-tightness. High purity oxygen (>99.995%) was used at a flow rate of about 50 mL min^{-1}. Up to six cell containers were connected in series using silicone tubes (Cole–Parmer Instrument co., Silicone Tubing (Platinum) L/S® 16) to flow the oxygen. The schematic of our experiment is shown in Fig. 1. Before testing, the cells were stabilized at open circuit for 10 h with flowing O_2. Electrochemical tests were performed at room temperature using a VMP3 cycler (Bio-Logic SAS). The cycle life was monitored at a constant current of 50 mA g^{-1}_{carbon} with voltage cut-off between 2.0 V and 4.3 V. The electrochemical impedance spectra were obtained in the frequency range from 200 kHz to 20 mHz with an amplitude of 5 mV. SEM observation was performed using a Hitachi S-4700 field emission gun scanning electron microscope (FEG-SEM). The Li sample was prepared in an Ar filled glove box and transferred to the FEG-SEM using a proprietary sample exchange holder that prevents air contamination between the glove box and the FEG-SEM. XRD was performed using a Rigaku table top X-ray diffractometer running at 600 W (X-ray

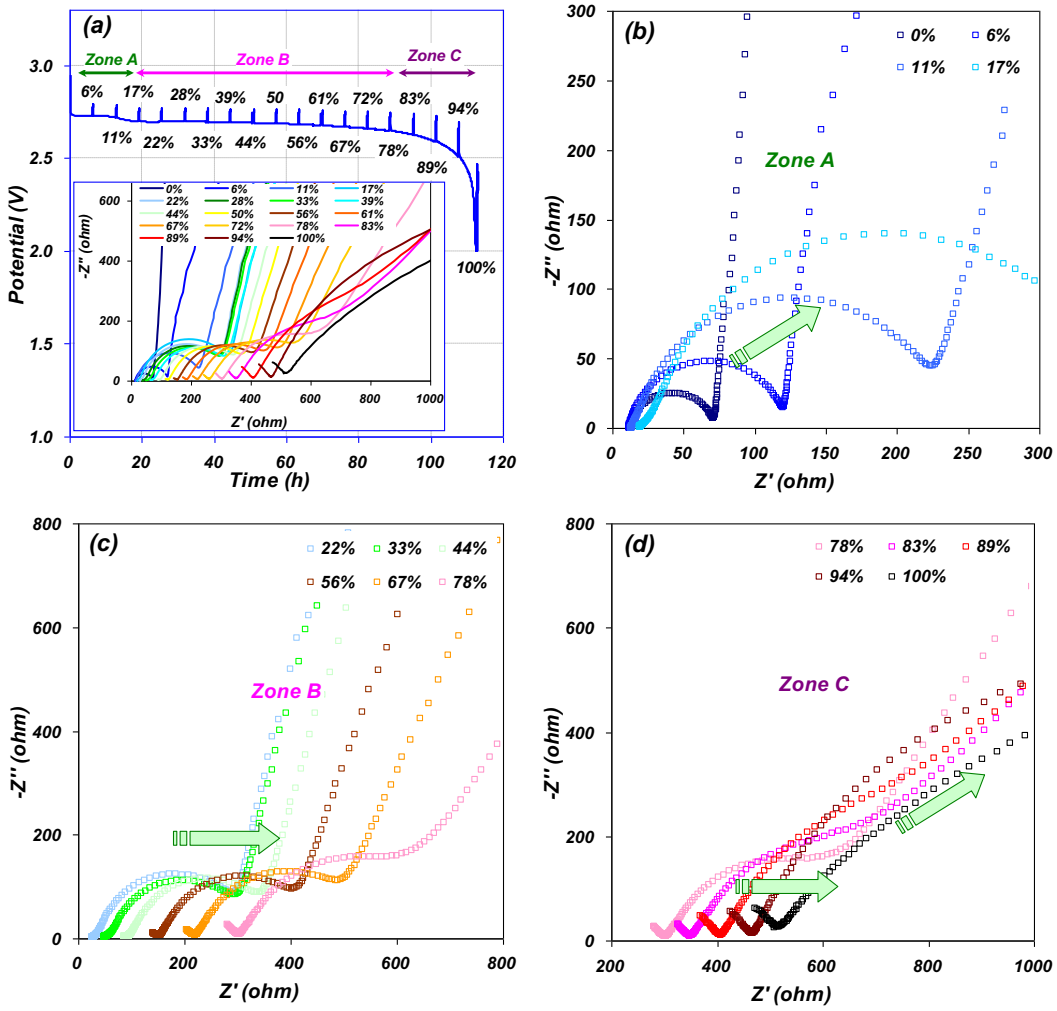

Fig. 4. (a) The first discharge profile of the 6th cell indicating the points of electrochemical impedance measurement. The pattern of impedance evolution can be categorized by (b) zone A showing the increase of Ri + Re without change of Rs, (c) zone B showing the increase of Rs with a negligible increase of Ri + Re, and (d) zone C showing the increase of Rs with a significant increase of Ri + Re (Rs: impedance from the ion conductivity in electrolyte, Ri: impedance from the interface film, Re: impedance from the charge transfer reactions).

tube) using Co Kα radiation (1.79Å). The XRD sample was prepared in an Ar filled glove box and analyzed in an air-tight sample holder. The moisture content in the cell containers and the atmosphere was measured by a dew point sensor (GE, M series sensor/Moisture Target Series 6).

3. Results and discussion

Fig. 2 shows the discharge profile of the 1st cycle according to the cell positions at a constant current for the cells sealed in the containers under flowing O_2 as shown in Fig. 1. Some voltage disturbance of the 2nd cell in Fig. 2 is perhaps owing to a bad contact within the cell. The dew point of the first container was −25 °C (*ca.* 500 ppm H_2O) and that of the 6th container was −15 °C (*ca.* 1500 ppm H_2O) under the environmental condition in the range of 0–20 °C dew point. It is evident in Fig. 2 that cell-to-cell deviation is more than 100% and there is a trend with the order of O_2 flow through the cells. The cells closer to the O_2 outlet show higher discharge capacity than those closer to the O_2 inlet-the 6th cell has 139% higher discharge capacity than the 1st cell. The inset of Fig. 2 shows that the ohmic resistance (Rs), contributed by the electrolyte, increases with the sequence of the cell connection and higher Rs values were found with the cell at the oxygen outlet. The weight change also shows the same trend-higher weight increase of the 6th cell (22 mg) cannot be explained by the oxygen uptake (3.3 mg) assuming all the discharge capacity comes from the formation of Li_2O_2. Similar results were reported regarding the increase of discharge capacity by some previous investigators [18–20]. In the gas containing 10% CO_2 in O_2, the 1st discharge capacity was about 60% higher than that of pure O_2 in dimethoxyethane (DME) [18]. In the other report, the 1st discharge capacity with 10% CO_2 was about 100% higher than that with pure O_2, and the capacity increased to 189% with 50% CO_2 in ethylene carbonate (EC) and diethyl carbonate (DEC) [19]. Meini et al. also reported that water had an effect on the discharge capacity [20]. They found that the cells exposed to water vapor and the cells that had a small leak to the ambient atmosphere showed higher discharge capacity than sealed Li-O_2 cells. Clearly, the accumulation of parasitic reactions is the reason for the increased discharge capacity according to the cell connection sequence.

Fig. 3 shows the discharge/charge profiles and the relevant impedance change observed at the end of the discharge and

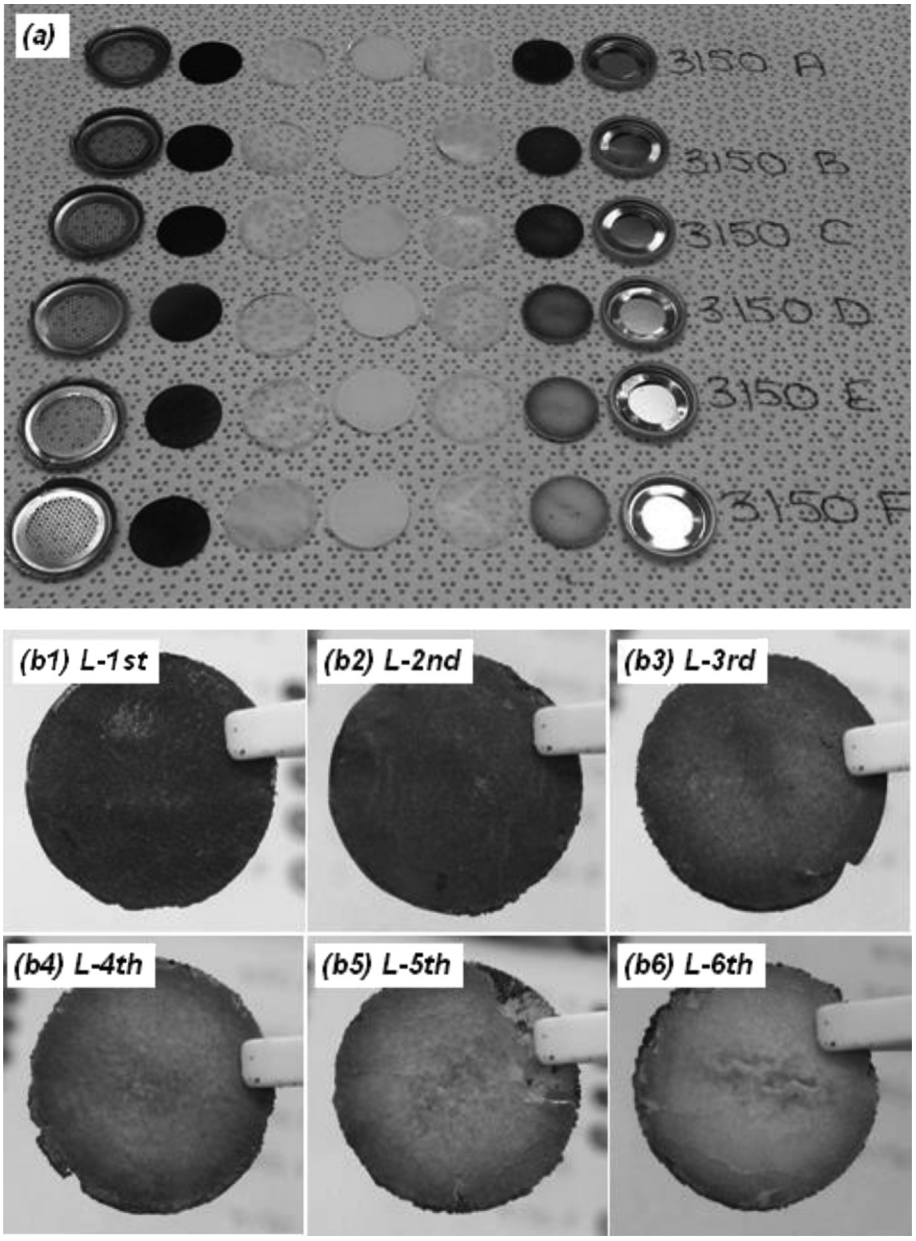

Fig. 5. Photographs of (a) disassembled cells and (b) lithium metal anodes after the 1st discharge. The Li metal surface turns black in the 1st cell and then turns to a thick white film in the 6th cell.

charge states for the first 2 cycles. The cells all showed significantly different impedance behavior arising from the cell connection sequences. In the 1st cell: Rs remains constant while [Ri + Re] gradually increased with cycles, where Ri is the impedance contribution from the interface film and Re arises from charge transfer reactions. On the other hand, in the 2nd and 3rd cells, Rs significantly increased with cycling. Especially in the 3rd cell, both Rs and [Ri + Re] increase rapidly with cycling. This result explicitly indicates the increase of contaminant accumulation in subsequent cells with inducing the dry-out of electrolyte. The increase of cell weight is more significant with cycling than the initial values in Fig. 2. After 10 cycles, the weight increases by −3.1 mg, 11.6 mg and 46.8 mg for the 1st cell, the 2nd cell and the 3rd cell respectively; the decreased weight of the 1st cell is probably due to the electrolyte evaporation surpassing the accumulated weight of by-products. The trend of weight increase indicates that the parasitic reactions are prolonged during the cycles.

A more detailed impedance study was carried out on the 6th cell due to its higher content of contaminants because of its place in the sequence. The evolution of the *in-situ* impedance spectra as a function of the depth of discharge (DOD) is shown in Fig. 4. The change of impedance spectra can be separated into 3 different zones categorized by the following DOD regions; 0–20%, 20–80% and 80–100%. In zone-A (Fig. 4b), [Ri + Re] increases without a change of the Rs, indicating that the electrolytes are relatively stable in the beginning of discharge and the reformation of passivation film leads the change of impedance in this zone. The similar phenomenon was reported by Meini et al. [20]; The [Ri + Re] increase by the formation of LiOH layer on the surface of

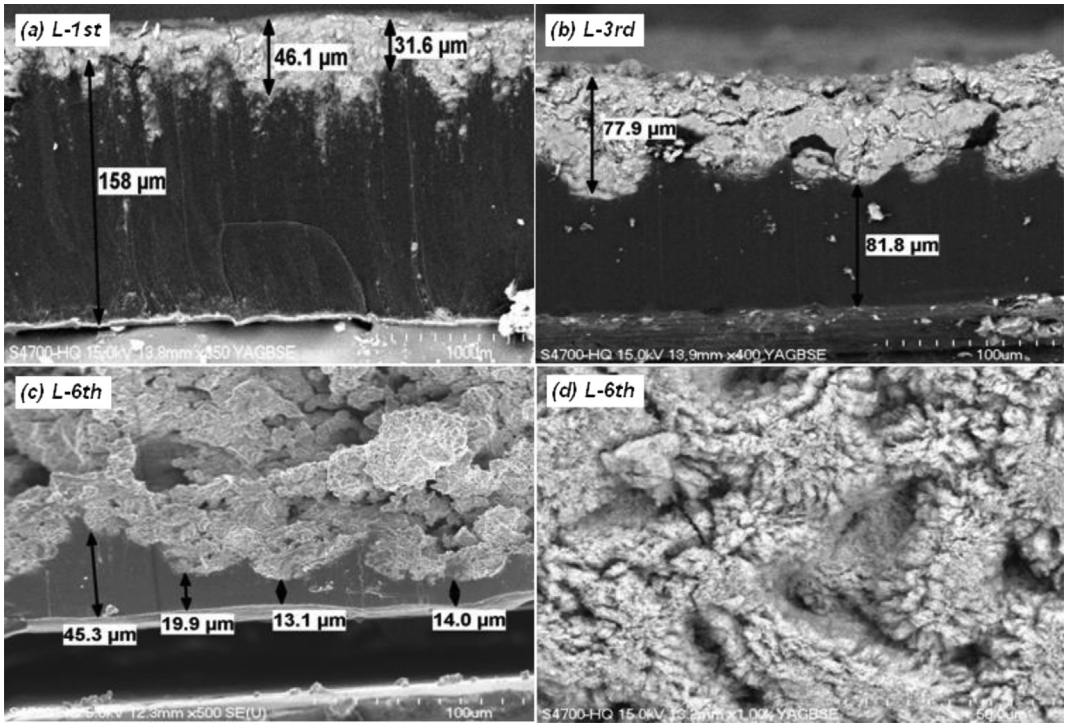

Fig. 6. SEM images of (a) ~ (c) the cross section of lithium metal anode after the 1st discharge and (d) the surface of lithium metal anode from the 6th cell. The arrows highlight the different thickness dimensions of the metallic lithium layer while the rough and porous surface layer grows according to the cell connection order.

lithium metal anode in the electrolyte containing 1000 ppm water. Zone-B (Fig. 4c) shows a significant increase of Rs with a negligible increase of [Ri + Re], which implies that the electrolyte decomposition is accelerated by the Li_2O_2 generation in the cathode side. Zone-C (Fig. 4d) shows the increase of Rs and [Ri + Re]. The increase of Rs is the extension of the electrolyte depletion in Zone-B, while the increase of [Ri + Re] represent the deterioration of electrode structure caused by the accumulation of the reaction products (Li_2O_2, LiOH, Li_2CO_3) on the electrodes.

In order to investigate the causes behind the trend of cell failure, post-mortem analysis was carried out on the six cells after the 1st discharge. Fig. 5 shows the optical photographs of the cell components (a) and lithium anodes (b). It is clearly seen that the Li surface is black in the 1st cell and the surface becomes covered with a thick white film in the 6th cell. The white film is believed to be responsible for the significant increase of the cell weight and the cell resistance. Assary et al. [21] reported the effect of oxygen crossover on the anode of a Li-O_2 battery and showed the similar phenomena on the lithium metal. However, it cannot explain the trend according to the cell connection sequences since all the cells are exposed to the same conditions of O_2-crossover.

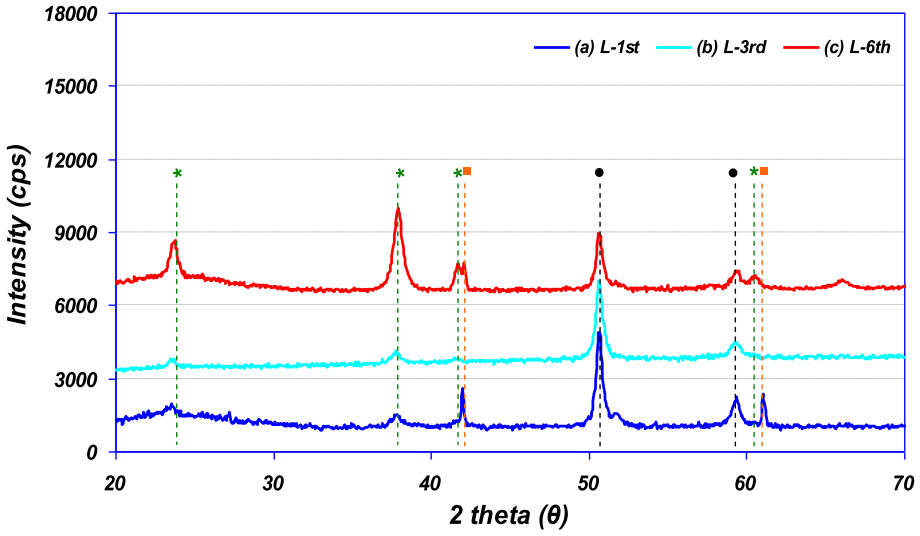

Fig. 7. XRD patterns of lithium metal anode after the 1st discharge. (*) LiOH, (■) lithium metal, (●) austenite from sample holder.

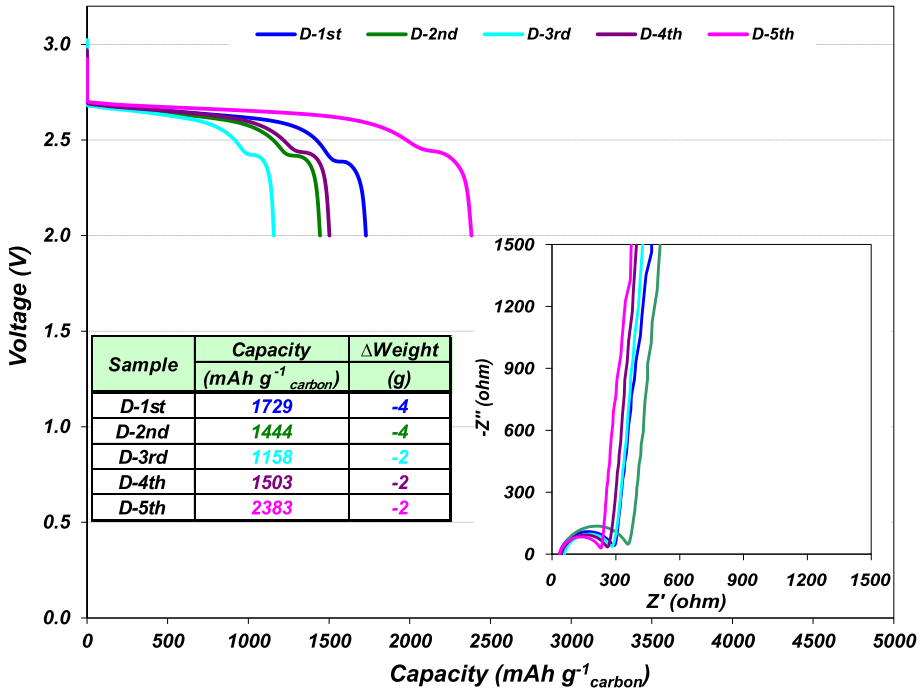

Fig. 8. The 1st discharge profiles according to the cell positions at a constant current of 50 mA g^{-1}_{carbon} between 2.0 and 4.3 V. Experiments conducted in the dry-room which was controlled to less than −40 °C dew point. The impedance profiles, the discharge capacity and the cell weight change after 1st discharge for each cell are in the inset.

Fig. 6 shows the SEM images of the cross-section of lithium metal anode after the 1st discharge. The thickness of the metallic lithium layer (compact black layer indicated by arrows) decreases with the cell connection sequences, and the Li metal surface becomes covered by porous and rough layers (which occupy more volume), as the cell is far down the connection sequence. The pores in the anode absorb the electrolyte from the separator layer and are responsible for the severe increase of Rs in Fig. 4. To identify the surface film, XRD analysis was performed on the surface of this layer. Fig. 7 shows that LiOH is the main component that grows with the descending cell connection sequences, which implies that the moisture contamination is leading the parasitic reactions in this experimental condition.

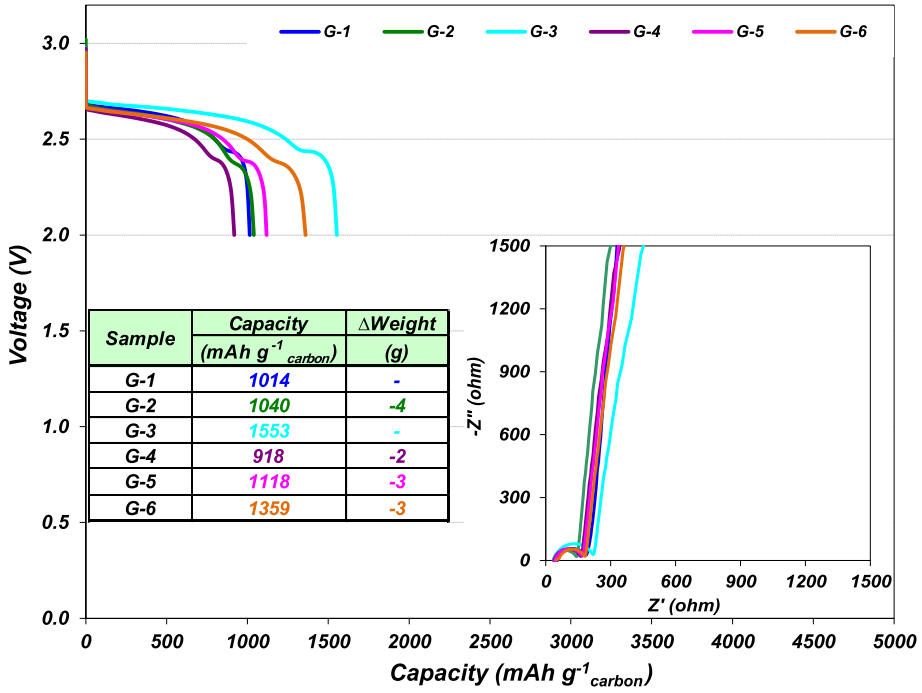

Fig. 9. The 1st discharge profiles according to the cell positions at a constant current of 50 mA g^{-1}_{carbon} between 2.0 and 4.3 V. Experiments conducted in the glove-box filled with helium which was controlled to less than −90 °C dew point. The table lists the 1st discharge capacity and the weight change after the 1st discharge. The impedance profiles for each cell, the discharge capacity and the cell weight change after 1st discharge are displayed in the inset.

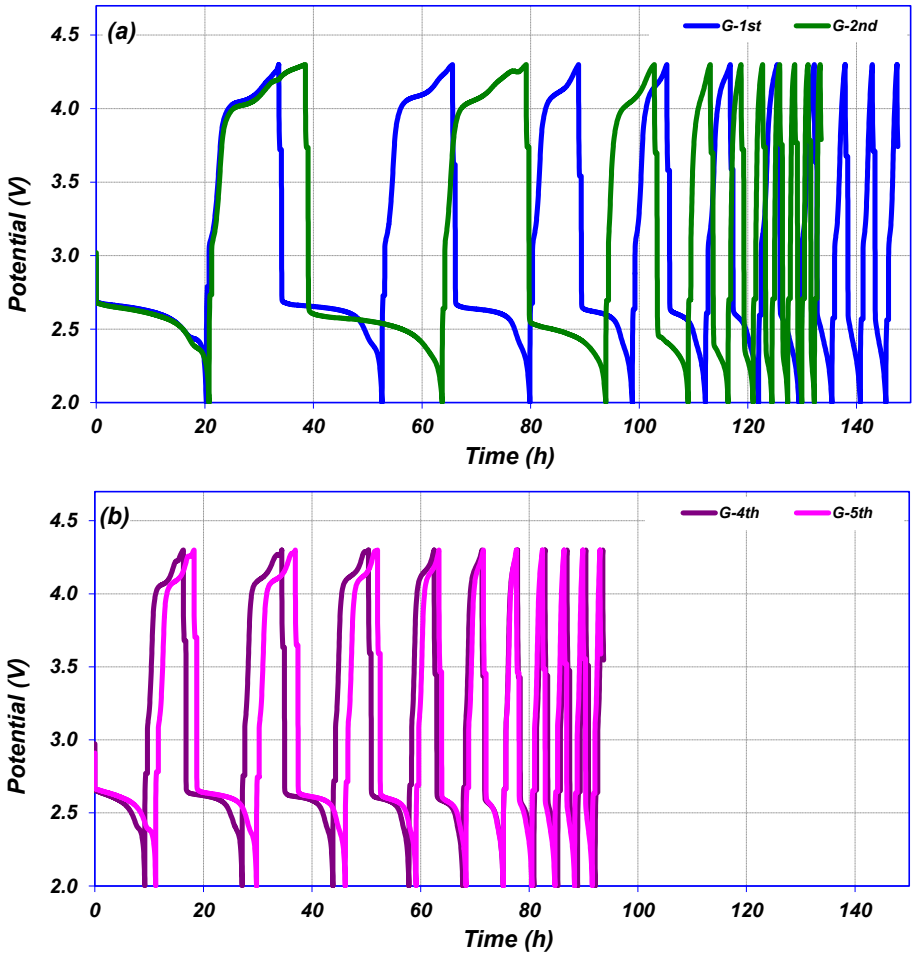

Fig. 10. Voltage profiles between 2.0 and 4.3 V for 10 cycles at current rates of (a) 50 mA g^{-1}_{carbon} and (b) 100 mA g^{-1}_{carbon} in the oxygen-filled container in the Helium-filled glove-box which are controlled to less than −90 °C dew point.

In this system, two kinds of parasitic reactions can be involved in the cell; the electrochemical reactions that can take place on the cathode electrode during the discharge, which contribute to the discharge capacity, and the chemical reactions that doesn't contribute to the cell capacity but deteriorate the performance of lithium anode. The additional capacity caused by H_2O can be described as below reactions [22];

$$2H_2O + 2Li^+ + 2e^- \rightarrow 2LiOH + H_2 \quad (1)$$

$$2H_2O + Li_2O_2 + 2Li^+ + 2e^- \rightarrow 4LiOH \quad (2)$$

The weight increase based on the above reactions is about 1.3 mg (calculated from the excess discharge capacity), which cannot explain the excessive increase of cell weight of 22 mg of the 6th cell in Fig. 2. This indicates that additional chemical reactions are involved in the cells, leading to the increase of cell weight and the serious damage on the cell performance. As evidenced by the analysis data on the lithium metal anode in Fig. 6, the parasitic reaction caused by H_2O is dominated by the following reaction [23];

$$2H_2O + 2Li \rightarrow 2LiOH + H_2 \quad (3)$$

The amount of lithium to yield the weight increase of 22 mg corresponds to 35% of lithium anode (200 μm thickness, 2 cm^2 dimension) based on the above reaction, which is reasonably in line with the result in Fig. 6.

To verify this observation, we set up the test cells in the dry-room which was controlled under −40 °C dew point. Fig. 8 represents the 1st discharge profile according to the cell positions, which is completely different from the previous results (Fig. 2). The weight of the cell and Rs impedance were found quite stable, while the discharge capacity does not show the correlation with the cell connection sequences.

When the cells are cycled in the glove box, where the moisture is controlled under −90 °C dew point, the 1st discharge profile is shown in Fig. 9. Unlike the previous tests where all the cell containers are connected in series with continuous flowing O_2, the cells are individually isolated and tested in the closed system after filling O_2. Under the O_2 flow condition (50 ml min^{-1}), the dew point in the containers was about −65 °C, which means that ~5 ppm H_2O is originated from the O_2 feed line. The figure shows that the 1st discharge capacity is less than the capacity in the dry room, and without an increase of the cell weight and Rs. This result demonstrates that the moisture from the atmosphere and O_2 feeding line is responsible for the significant increase of the cell weight, cell resistance and 1st discharge capacity in Fig. 2.

Fig. 10 shows the voltage profiles for the 10 cycles with different current rate in the He filled glove-box. The cycle life is improved but still too short to be useful for practical applications. The impedance measured for 10 cycles are shown in Fig. 11. The plots measured at the end of each discharge (a) and at the end of each charge (b) are totally different from those previous obtained under ambient conditions without moisture control (Fig. 3b, d and f). Even when

the capacity retention is less than 20% after 10 cycles, the impedance profiles are well maintained in the frequency range between 200 kHz and 20 mHz. The lower frequency behavior is currently under investigation to further understand this phenomenon. To analyze the different behavior according to the cell connection environment, we did the post-mortem analysis again, and the optical photographs of the lithium surface are showed in Fig. 12. In both cases, after the 1st discharge in the dry-room (a) and after 10 cycles in the glove-box (b), the Li metal anodes remained shiny without surface changes during the test period of 100 h.

4. Conclusions

In this study, we examined lithium-air cells under different experimental conditions with respect to moisture contamination. We performed electrochemical measurements, electrochemical impedance spectroscopy and post-mortem analysis to understand the effects of moisture contamination by investigations of a sealed container in an ambient atmosphere *vs.* sealed container in a dry-room or in a glove-box. The cells tested in the sealed container in ambient atmosphere showed higher discharge capacity, higher impedance and significant weight gain after the 1st discharge to 2.0 V under O_2 flow. On the other hand, the cells tested in the dry-room or glove-box showed less discharge capacity, negligible impedance change and insignificant cell weight change. It is believed that the contaminated gas causes parasitic reactions in the downstream neighboring cells. Post-mortem analysis revealed that the deterioration of lithium metal anode leads to the cell failure, which is directly related to the moisture contamination. This finding supports the idea that protection of the lithium metal electrode is crucial to realize the practical applications of Li-O_2 or Li-air batteries. We confirmed that the performance of Li-O_2 batteries is very sensitive to even trace amounts of moisture contamination. Furthermore, we found that every single part of cell design including the choice of fitting parts and water permeability of fitting material should be verified to obtain credible results.

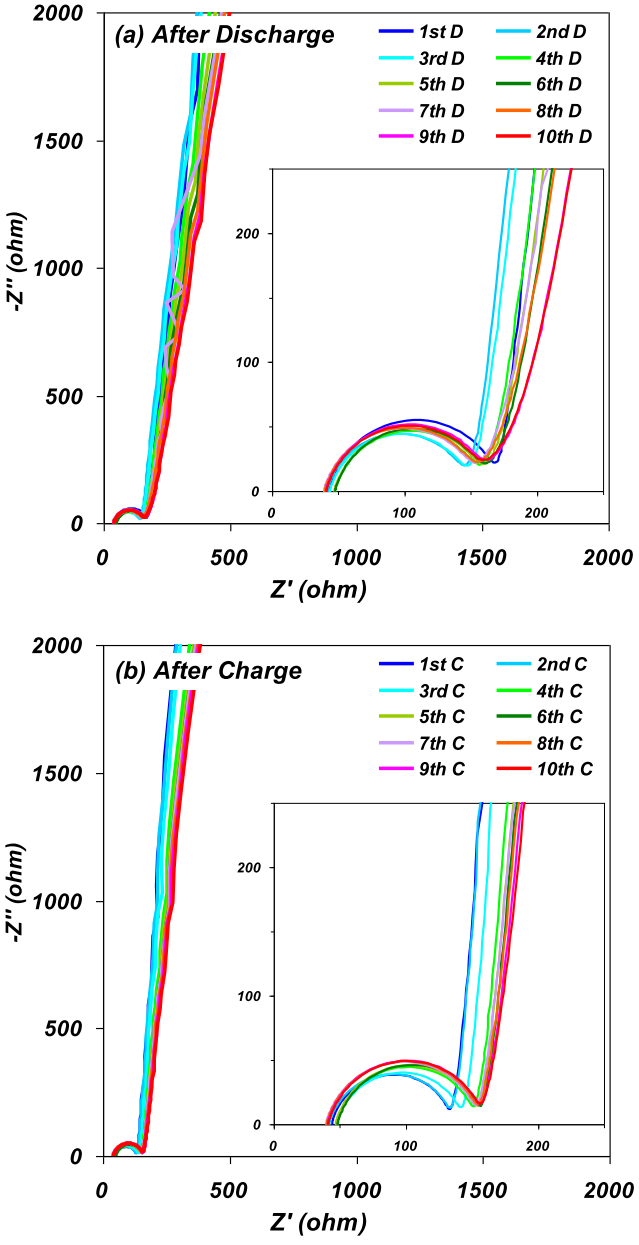

Fig. 11. Nyquist plots after (a) discharge and (b) charge during 10 cycles.

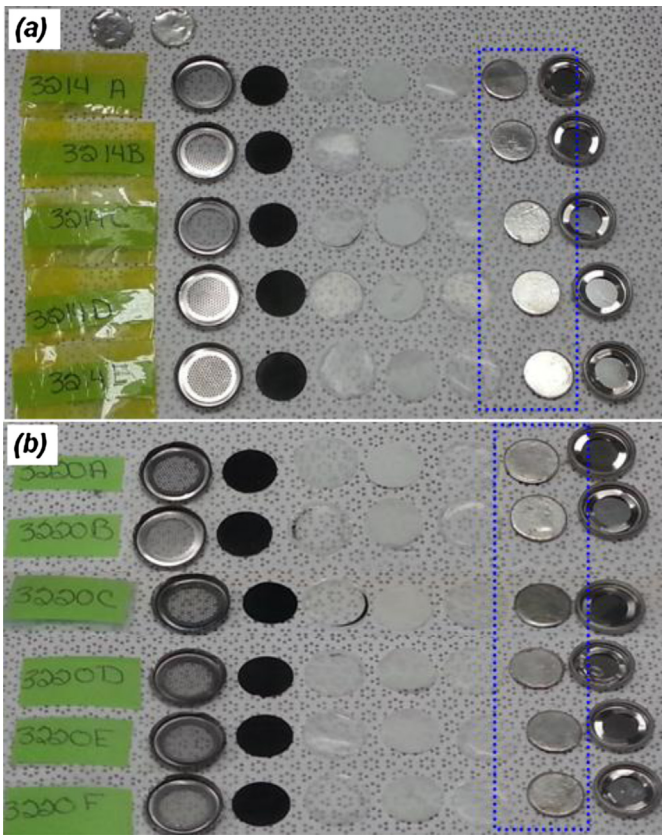

Fig. 12. Photographs of disassembled cells after (a) the 1st discharge in the dry-room and (b) the 10 cycles in the glove-box. All the lithium metal anodes remain shiny unlike the lithium metal anode discharged in the sealed container in the ambient atmosphere.

References

[1] J. Hou, M. Yang, M.W. Ellis, R.B. Moore, B. Yi, Phys. Chem. Chem. Phys. 14 (2012) 13487–13501.
[2] J. Christensen, P. Albertus, R.S. Sanchez-Carrera, T. Lohmann, B. Kozinsky, R. Liedtke, J. Ahmed, A. Kojic, J. Electrochem. Soc. 159 (2012) R1–R30.
[3] P.G. Bruce, S.A. Freunberger, L.J. Hardwick, J.M. Tarascon, Nat. Mat. 11 (2012) 19–29.
[4] W. Xu, J. Hu, M.H. Engelhard, S.A. Towne, J.S. Hardy, J. Xiao, J. Feng, M.Y. Hu, J. Zhang, F. Ding, M.E. Gross, J.G. Zhang, J. Power Sources 215 (2012) 240–247.

[5] B.D. McCloskey, D.S. Bethune, R.M. Shelby, T. Mori, R. Scheffler, A. Speidel, M. Sherwood, A.C. Luntz, J. Phys. Chem. Lett. 3 (2012) 3043–3047.
[6] Y. Chen, S.A. Freunberger, Z. Peng, F. Bardé, P.G. Bruce, J. Am. Chem. Soc. 134 (2012) 7952–7957.
[7] M.J. Trahan, S. Mukerjee, E.J. Plichta, M.A. Hendrickson, K.M. Abraham, J. Electrochem. Soc. 160 (2013) A259–A267.
[8] Y. Cui, Z. Wen, X. Liang, Y. Lu, J. Jin, M. Wu, X. Wu, Energy Environ. Sci. 5 (2012) 7893–7897.
[9] H.D. Lim, K.Y. Park, H. Song, E.Y. Jang, H. Gwon, J. Kim, Y.H. Kim, M.D. Lima, R.O. Robles, X. Lepró, R.H. Baughman, K. Kang, Adv. Mat. (2013) 1–5.
[10] J.J. Xu, D. Xu, Z.L. Wang, H.G. Wang, L.L. Zhang, X.B. Zhang, Angew. Chem. Int. Ed. 52 (2013) 1–5.
[11] B.D. McCloskey, R. Scheffler, A. Speidel, D.S. Bethune, R.M. Shelby, A.C. Luntz, J. Am. Chem. Soc. 133 (2011) 18038–18041.
[12] H.G. Jung, Y.S. Jeong, J.B. Park, Y.K. Sun, B. Scrosati, Y.J. Lee, ACS Nano. 7 (2013) 3532–3539.
[13] R. Black, J.H. Lee, B. Adams, C.A. Mims, L.F. Nazar, Angew. Chem. Int. Ed. 52 (2013) 392–396.
[14] Y. Cui, Z. Wen, Y. Lu, M. Wu, X. Liang, J. Jin, J. Power Sources 244 (2013) 614–619.
[15] A. Zhamu, G. Chen, C. Liu, D. Neff, Q. Fang, Z. Yu, W. Xiong, Y. Wang, X. Wang, B.Z. Jang, Energy Environ. Sci. 5 (2012) 5701–5707.
[16] I.C. Jang, Y. Hidaka, T. Ishihara, J. Power Sources 244 (2013) 606–609.
[17] H.G. Jung, J. Hassoun, J.B. Park, Y.K. Sun, B. Scrosati, Nat. Chem. 4 (2012) 579–585.
[18] S.R. Gowda, A. Brunet, G.M. Wallraff, B.D. McCloskey, J. Phys. Chem. Lett. 4 (2013) 276–279.
[19] K. Takechi, T. Shiga, T. Asaoka, Chem. Commun. 47 (2011) 3463–3465.
[20] S. Meini, M. Piana, K. Tsiouvaras, A. Garsuch, H.A. Gasteiger, Electrochem. Solid State Lett. 15 (2012) A45–A48.
[21] R.S. Assary, J. Lu, P. Du, X. Luo, X. Zhang, Y. Ren, L.A. Curtiss, K. Amine, ChemSusChem 6 (2013) 51–55.
[22] D. Pletcher, J.F. Rohan, A.G. Ritchie, Electrochim. Acta. 39 (1994) 1369–1376.
[23] K. Chen, Z. Zhang, E. Ni, J. Appl. Electrochem. 40 (2010) 197–204.